A Survey of Fractional-Order Circuit Models for Biology and Biomedicine

Todd J. Freeborn, *Student Member, IEEE*

***Abstract*—In this survey, we present many of the fractional-order circuit models used in biomedicine and biology to fit experimentally collected impedance data. An overview of the different methods used to extract the impedance parameters from collected datasets are also presented. Applications of fractional order circuit models for modelling human tissue, plant physiology, respiratory systems, and tissue–electrode interfaces are presented to highlight the significance of these models and their potential for further research. This survey is of a tutorial nature intended as an introduction to fractional-order circuit models and to consolidate the many models reported across literature.**

***Index Terms*—Bioimpedance, fractional calculus.**

I. Introduction

FRACTIONAL calculus, the branch of mathematics regarding differentiations and integrations to noninteger orders, is a field that is over 300 years old [1]. Its origins dating back to a correspondence from 1695 between Leibnitz and L'Hôpital, with L'Hôpital inquiring about Leibnitz's notation, $d^n y/dx^n$, and the meaning if $n = 1/2$. The reply from Leibnitz, "It will lead to a paradox, a paradox from which one day useful consequences will be drawn, because there are no useless paradoxes," [2] has proven him quite the prophet. The last few decades has seen an explosion of applications of fractional calculus in many fields of science and engineering [3], [4].

A fractional derivative of order α is given by the Caputo derivative [6] as

$$ {}_a^C D_t^\alpha f(t) = \frac{1}{\Gamma(\alpha - n)} \int_a^t \frac{f^{(n)}(\tau) d\tau}{(t-\tau)^{\alpha+1-n}} \tag{1} $$

where $\Gamma(\cdot)$ is the gamma function and $n - 1 \leq \alpha \leq n$. We use the Caputo definition of a fractional derivative over other approaches because the initial conditions for this definition take the same form as the more familiar integer-order differential equations. Applying the Laplace transform to the fractional derivative of (1) with lower terminal $a = 0$ yields

$$ \mathscr{L}\{{}_0^C D_t^\alpha f(t)\} = s^\alpha F(s) - \sum_{k=0}^{n-1} s^{\alpha-k-1} f^{(k)}(0). \tag{2} $$

Therefore, it becomes possible to define a general fractance device with impedance proportional to s^α [7] where the traditional circuit elements are special cases of the general device when the order is $-1, 0$, and 1 for a capacitor, resistor, and inductor, respectively. A special case of the general fractance device is referred to as a constant phase element (CPE), with impedance $Z_{\mathrm{CPE}} = 1/(j\omega)^\alpha C$ or $1/s^\alpha C$ in the s-domain, where C is the capacitance and α is its order. It's name is in reference to the phase angle, ϕ_{CPE}, which is independent of frequency and dependent only on the order, α, given as $\phi_{\mathrm{CPE}} = \alpha\pi/2$. While $\alpha \in \Re$ is mathematically possible, the values from experimentally collected data are typically in the range of $0 < \alpha < 1$. For reference, the bode plots of s^α when $\alpha = 0.2$, 0.4, 0.6, 0.8, and 1 are given in Fig. 1. These devices have also been called fractional capacitors, in reference to their order which takes a value between the traditional circuit elements of a resistor and capacitor. It is for this reason that we use a capacitor as the schematic representation of CPEs in this work. These CPEs have shown numerous applications in the field of bioimpedance, which measures the passive electrical properties of biological materials. These measurements give information about the electrochemical processes in tissues and can be used to characterize the tissue or monitor for physiological changes [8]. In this survey, we present many of the fractional

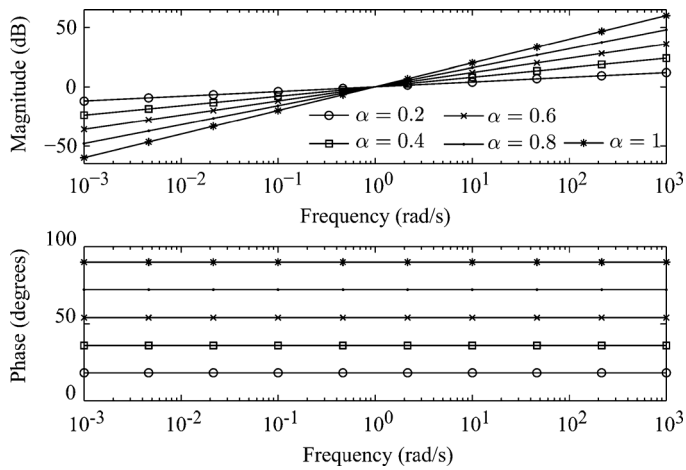

Fig. 1. Bode plots of s^α when $\alpha = 0.2, 0.4, 0.6, 0.8$, and 1.

Manuscript received December 21, 2012; revised March 27, 2013; accepted April 22, 2013. Date of publication June 12, 2013; date of current version September 09, 2013. This work was supported by Canada's National Sciences and Engineering Research Council (NSERC), Alberta Innovates—Technology Futures, and Alberta Advanced Education and Technology through graduate student scholarships. This paper was recommended by Guest Editor A. Elwakil.

The author is with the Department of Electrical and Computer Engineering, University of Calgary, Calgary, AB, T2N 1N4 Canada (e-mail: tjfreebo@ucalgary.ca).

Color versions of one or more of the figures in this paper are available online at http://ieeexplore.ieee.org.

Digital Object Identifier 10.1109/JETCAS.2013.2265797

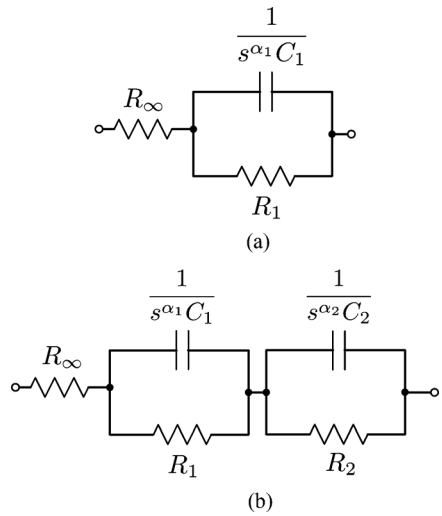

Fig. 2. Theoretical (a) single and (b) double dispersion Cole impedance models.

circuit models used in biomedicine and biology to fit experimentally collected impedance data. An overview of the different methods used to extract the impedance parameters from collected datasets are also presented. Applications of fractional order circuit models for modelling human tissue, plant physiology, respiratory systems, and tissue–electrode interfaces are presented to highlight the significance of these models and their potential for further research. An example of an extraction of the fractional impedance parameters from an impedance dataset using MATLAB is given. A comparison of the fractional-order impedance models with their impedance plots are presented to aid in selecting which model to use. This survey is of a tutorial nature intended as an introduction to fractional-order circuit models and to consolidate the many models reported across literature.

II. Cole Impedance Models

In the field of bioimpedance measurements the Cole impedance model, introduced by Kenneth Cole in 1940 [9], is widely used for characterizing biological tissues and biochemical materials. In literature, this model has also been commonly referred to as the Cole-Cole model or Cole-Cole impedance model. However, the Cole-Cole model is actually a similar model introduced by the Cole brothers in 1941 regarding dielectric permittivity [10]. Therefore, care needs to be taken when describing the model to prevent confusion between work with dielectric permittivity and impedance.

The Cole model, shown in Fig. 2(a), is composed of three hypothetical circuit elements. A high-frequency resistor R_∞, a resistor R_1 and a CPE. The impedance of this model is then given by

$$Z(s) = R_\infty + \frac{R_1}{1 + s^{\alpha_1} R_1 C_1} = Z' + jZ''. \tag{3}$$

Noting that $s^\alpha = (j\omega)^\alpha = \omega^\alpha [\cos(\alpha\pi/2) + j\sin(\alpha\pi/2)]$. This model has become very popular because of its simplicity and good fit with measured data, illustrating the behavior of impedance as a function of frequency. However, while this model is effective at representing experimentally collected bioimpedance data, it does not provide an explanation of the underlying mechanisms. Physiologically, the resistances in this model are contributed by the numerous intracellular, extracellular, and cellular membrane resistances within the tissue; with capacitance contributed by the membrane capacitances of the numerous tissue cells. The parameter α is a dimensionless quantity known as the dispersion coefficient. It is possible to regard it in several ways, including, as a distribution of relaxation times caused by the heterogeneity of cell sizes and shapes, a measure of the deviation from an ideal capacitor in the equivalent circuit, or as a measure of physical processes like the Warburg diffusion [8].

Now, while these models do not provide an explanation of the underlying mechanisms, there has been a large and expanding body of research regarding their use in many diverse fields of biology and biomedicine. The single dispersion model and its parameters have been investigated for applications in biomedicine that include:

- characterizing muscle, liver, lung, and spleen tissues excised from sheep [11];
- estimating the hemocrit value or total volume of red blood cells in a sample of human blood [12] or assessing the quality of red blood cell suspensions under storage [13];
- monitoring tissue ischemia, the condition of insufficient oxygen and nutrient supply, from pH value estimated from the impedance parameters [14];
- monitoring intra/extra-cellular volume or detecting tissue structural alterations through the α parameter, also referred to as the bioimpedance width [15];
- monitoring the hydration process of patients during haemodialysis as a potential indicator of hypotension crisis [16];
- accurate modelling of different types of human skulls for simulation of their properties for bioelectric related research [17];
- usefulness of the impedance parameters for estimating tissue response to chronic microelectrode arrays [18];
- detection of occlusal noncaviated carious for dentistry [19];
- body composition analysis for total body water, extracellular fluid content, intracellular fluid content, and fat mass [20].

Many investigations regarding the Cole parameters and their relation to cancerous tissues have been conducted with applications that include:

- aiding in the diagnosis of cervical cancer in women [21];
- classifier based diagnostic tool for healthy and cancerous hepatic tissue in humans [22];
- identifying cancer [23] and the features of surrounding areas in breast tissue [24];
- minimally invasive detection of bladder cancer [25];
- as a diagnostic and prognostic factor for survival in cancer patients [26].

An expanded model, the double dispersion Cole model, is used to accurately represent the impedance over a larger frequency range or for more complex materials. This model, shown in Fig. 2(b), is composed of an additional parallel combination

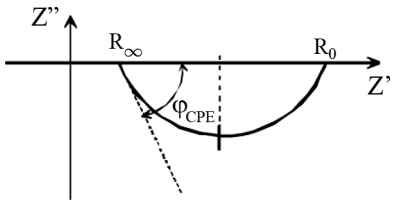

Fig. 3. Impedance loci used to graphically extract the single dispersion Cole impedance parameters.

of a resistor and CPE in series with the single dispersion Cole model with total impedance given by

$$Z(s) = R_\infty + \frac{R_1}{1 + s^{\alpha_1} R_1 C_1} + \frac{R_2}{1 + s^{\alpha_2} R_2 C_2}. \quad (4)$$

The double dispersion Cole model and its parameters have been investigated for applications in:

- characterizing intestinal tissue excised from sheep [11];
- monitoring necrosis of human tumor xenografts during and/or after hyperthermia treatment [27];
- investigating the age-related changes of human dentine with potential to create nondestructive test methods applied to early caries and micro-leakage identification [28].

A. Cole Model Extraction Methods

To characterize a particular tissue or material using the single or double dispersion Cole models requires the determination of the four (R_∞, R_1, C_1, α) or seven (R_∞, R_1, R_2, C_1, C_2, α_1, α_2) parameters, respectively. Early methods extracted the parameters graphically from an impedance plot relating the imaginary impedance, Z'', to the real impedance, Z'. An example impedance loci used to extract the single dispersion Cole impedance parameters is shown in Fig. 3. From the circular arc the theoretical low frequency resistance, R_o, and high frequency resistance, R_∞, can be directly measured (see Fig. 3) where $R_1 = R_o - R_\infty$. The CPE order, α, can be calculated from the measured angle $\phi_{\rm CPE}$ through the relation $\phi_{\rm CPE} = \alpha\pi/2$. While the frequency at which $|Z''|$ has its maximum is equal to $1/\tau$ and the dispersion time constant is given as $\tau = [(R_o - R_\infty)\, C]^{1/\alpha}$, enabling the calculation of C with the previously measured parameters (R_o, R_∞, α). The double dispersion Cole parameters can be extracted in a similar fashion, with two circular arcs appearing in the impedance loci as a result of the two dispersions.

With the rise of computers and very powerful numerical fitting software such as LEVM/LEVMW [29] and MATLAB [30], the majority of parameters are now estimated using nonlinear least squares routines fitting experimental data to the desired model. Parameters are selected such that the least squares error between the experimental data and estimated response are minimized. While these fitting processes were initially applied to impedance data, research has been expanded to extract the parameters without requiring direct measurement of the impedance. Instead, parameters are extracted only from the real part of the impedance (Z')[31], [32], the imaginary (Z''), or the modulus [20], [32], [33] components of the impedance and even from time domain step response datasets [34]. Methods without requiring fitting routines have also been investigated to extract the parameters from the magnitude response [35], [36] and the time domain response to a triangle-wave current input [37].

A significant motivation in the research of alternative methods for extracting the impedance parameters is to reduce the amount of hardware and cost of instruments for these measurements [20]. Traditionally, to collect the impedance data requires an impedance analyzer which is expensive and not portable. Low-cost hardware to accomplish this same task was reported in [25], [38]. Lowering the cost of instruments that extract the Cole parameters without requiring direct measurement of the impedance has the potential to significantly reduce the barriers to conduct research especially with regards to real-time monitoring with portable devices [39].

III. Fractional Plant Models

Fractional impedance models are not only important in biomedicine but have shown useful applications in biology, specifically in regards to plant physiology. The single dispersion Cole model and its parameters have been investigated for:

- characterizing the tissues of different fruits and vegetables including apples, apricots [35], plumbs [36], potatoes, kiwis [35], [40], garlic, tomatoes, and pears; with potential to measure the maturity or give an estimate of lifespan for storage purposes [41];
- relationship between the rooting ability and Cole parameters of shoots and leaves of olive cuttings [42];
- effects of drying and freezing-thawing treatments on eggplant pulp samples [43];
- nondestructive method for detection of incipient mould development on wood surfaces [44];
- fit the impedance data collected from the bark and wood of current and one year old Scots pine shoots [45].

In [45], the single dispersion Cole model provided a more accurate fit with experimental data than two other integer circuit models for bark and wood, even when both integer models had more parameters (5 and 9, respectively) than the fractional model (3). For comparison, the integer order models are given in Fig. 4(a) and (b). This study concluded that the fractional model is better suited to model tissues with numerous types of cells with different sizes and morphologically different structures [45]. The double dispersion Cole model has also been investigated as an indicator of frost hardiness in Scots pine shoots [46].

The Cole impedance models are not the only fractional impedance models useful in matching the impedance data collected from plant tissues. The model, shown in Fig. 5, is composed of three resistors and three CPEs with impedance given by

$$Z(s) = R_\infty + \frac{R_1}{1 + s^{\alpha_1} R_1 C_1} + \frac{R_2}{1 + s^{\alpha_2} R_2 C_2} + \frac{1}{s^{\alpha_3} C_3} \quad (5)$$

is used to fit the impedance data collected from root/stem/electrode interface of willows to monitor the root growth through the change in the impedance parameters [47]. This method was investigated as a method of measuring root growth with the resistances $(R_1 + R_2)$ showing the highest correlation with the root

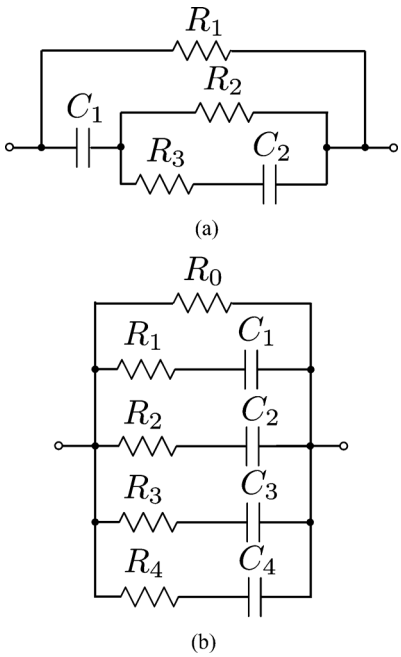

Fig. 4. Lumped circuits for modelling (a) bark and (b) wood to compare against a fractional circuit model in [45].

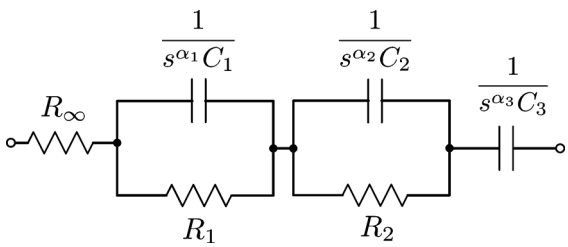

Fig. 5. Fractional impedance model to fit root/stem/electrode interface of willows grown to monitor root growth in [47].

fresh mass. This study also concluded that the speed and nondestructive nature of the measurements warranted further study on the effects of soil type, moisture content, and electrode position on the impedance parameters.

The model given in Fig. 6 composed of two CPEs and a resistor with impedance given by

$$Z(s) = \frac{1}{s^{\alpha_1}C_1} + \frac{R_2}{1 + s^{\alpha_2}R_2C_2} \tag{6}$$

is used to fit the impedance data collected from a wood sample to estimate the internal moisture gradients [48]. For this study, a portable device with applications to optimize wood drying, condition surveys of wood buildings and construction, and estimates of pulpwood moisture gradients was developed [48]. This portable device as well as others developed to extract the Cole parameters from plants and trees without requiring the use of an impedance analyzer [49], [50] creates the potential for extensive field studies in wood research not possible using traditional laboratory equipment.

IV. Electrode–Tissue Interface Model

Modeling the electrode–tissue interface is important for all systems involving biopotential recordings and stimulations.

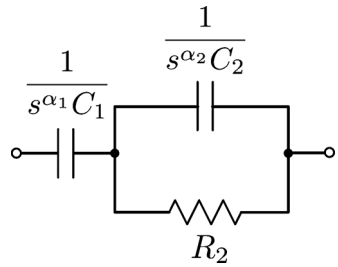

Fig. 6. Fractional order model to analyze moisture gradients of wood in [48].

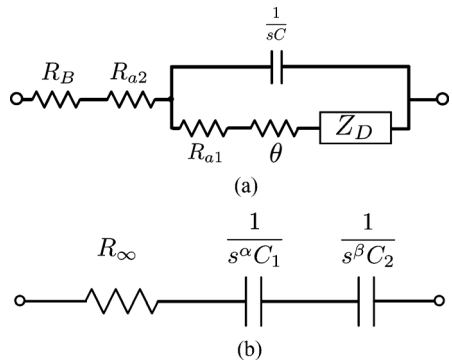

Fig. 7. (a) Tissue–electrode circuit model for a unit surface area [51] and (b) simplified distributed fractional order model [52].

This is even more important for pacemakers because device failures are often the result of properties of the electrode–tissue interface rather than component failure intrinsic to the device [51] with reported failures by commercial devices highlighting the need for more accurate models to ensure patient safety [52]. An equivalent fractional order circuit model of the electrode–tissue interface in living hearts was proposed in [51], shown in Fig. 7(a), that describes the impedance for a unit surface area. This model was derived from experimentally collected data of perfused living rat hearts and is composed of 6 elements to describe the behavior of the tissue–electrode interface. R_B is the bulk tissue resistance, R_{a1} and R_{a2} are the electrode access resistances, θ is the electrochemical charge transfer resistance, C is the dipole layer capacitance, and Z_D is a spatially confined Warburg impedance (CPE with $\alpha = 0.5$). It was recently proposed in [52] that the experimental data of the model in Fig. 7(a) could also be represented by the fractional order model given in Fig. 7(b); reducing the model to three elements, a resistance in series with two CPEs with impedance given by the expression

$$Z(s) = R_\infty + \frac{1}{s^{\alpha}C_1} + \frac{1}{s^{\beta}C_2}. \tag{7}$$

Though in reducing the electrode–tissue interface from that shown in Fig. 7(a) to that in (b) we lose the physiological description of each contributing element of the impedance; still the simplified model provides a good fit to the experimental data. Fractional models are also useful in simulations of the electrode–tissue interface and are relevant to biosensors, chronic indwelling electrodes, and cardiac pacemakers [51]–[53].

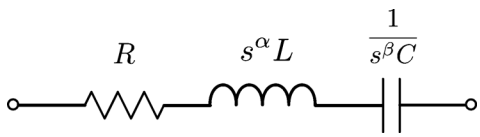

Fig. 8. Fractional order impedance model of the respiratory system of humans proposed in [59].

V. Fractional Respiratory Model

Fractional order models have been shown useful in modeling the mechanical impedance of the respiratory system in dogs [57], cats [58], and humans [59]. Many of these fractional-order models are based on the fractal structure of these physical systems [54], [55] which are very complex geometric systems [56]. An electrical equivalent representation of the mechanical impedance of the human respiratory system, given in Fig. 8, is composed of series connection of three elements. The impedance of this system is given by the expression

$$Z(s) = R + s^\alpha L + \frac{1}{s^\beta C} \tag{8}$$

where R is a Newtonian resistance, L the inertance, and C the compliance. This model is unique in that it introduces a fractional element, with impedance $Z_L = s^\alpha L$, different than the CPE's previously described. Where the order of the previous CPE's places them between the traditional elements of a resistor and capacitor, the order of this element places it between a resistor and inductor. It is for this reason that we use an inductor as the schematic representation of this element in Fig. 8 and could also refer to this element as a fractional inductor.

This model has been verified in both frequency and time domains to reasonably fit the experimentally collected data using the forced oscillation technique to measure the respiratory impedance. These impedance parameters are potentially useful in tuning controllers to deliver the reference pressure value and obtain optimal ventilation for a patient requiring minimal breathing effort yielding improvements to ventilatory assisting devices [59].

It has been shown in [60] that changes in the mechanical properties of lung parenchyma can be detected in the impedance parameters between healthy patients and those with chronic pulmonary disease. This model is able to capture the viscoelastic changes of soft tissues in the lungs. It has further been shown in [61] that the fractional order behavior observed in the respiratory input impedance is dependent on not only the tissue viscoelasticity, but also on the intrinsic geometry and morphology of the respiratory tree. The fractional model of Fig. 8 has also been used to investigate the respiratory mechanics in total liquid ventilation [62]. The fractional values were acknowledged to best explain the frequency-dependence of the input impedance with useful applications for the design of a pressure controller for total liquid ventilators and monitoring patient respiratory parameters during treatment.

VI. Simulation

While fractional order circuit models show a significant number of applications in biomedicine and biology, there are a lack of simulation tools to aid in the simulation of fractional order systems. Fractional circuit models are not currently supported by circuit simulation software packages and instead require integer order approximations typically realized using *RC* ladder topologies [63], [64]. There are many methods to realize approximations of CPEs that include continued fraction expansions (CFEs) and rational approximation methods [65]. The circuit to realize a fourth-order approximation of a CPE using the CFE method in [66] is given in Fig. 9. The magnitude and phase of the ideal (solid line) and fourth-order approximated (dashed) CPE with capacitance $12.6\ \mu$F and order $\alpha = 0.5$, shifted to a center frequency of 1 kHz, are presented in Fig. 10. From this figure we observe that the approximation is very good over almost four decades, from 200 Hz to 70 kHz, for the magnitude and almost two decades, from 200 Hz to 6 kHz, for the phase. In these regions, the deviation of the approximation from ideal does not exceed 1.23 dB and 0.23° for the magnitude and phase, respectively. The accuracy and bandwidth of the approximated CPEs can be increased by increasing the order of the approximation.

While there are no fractional order circuit models in SPICE to simulate biological tissues, the *Bioimpedance Simulator* software [67] is available to aid in simulations. This software package generates SPICE netlists to approximate the electrical

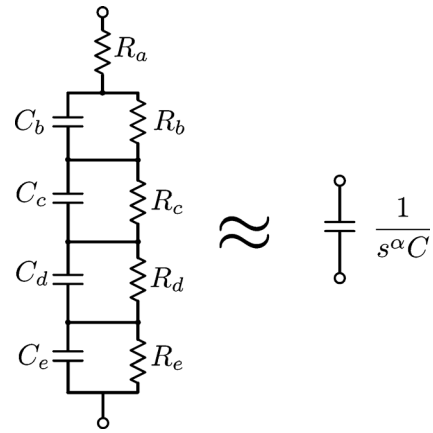

Fig. 9. *RC* ladder circuit to realize a fourth-order approximation of a CPE.

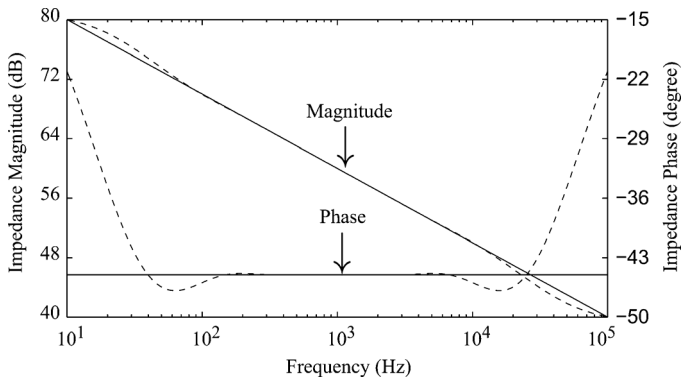

Fig. 10. Magnitude and phase response of an approximated CPE (dashed) compared to the ideal (solid) with $C = 12.6\ \mu$F and $\alpha = 0.5$ after scaling to a center frequency of 1 kHz ($R_a = 111.1\ \Omega$, $R_b = 251.7\ \Omega$, $R_c = 378.7\ \Omega$, $R_d = 888.9\ \Omega$, $R_e = 7369.7\ \Omega$, $C_b = 68.9$ nF, $C_c = 296$ nF, $C_d = 537$ nF, $C_e = 695$nF) .

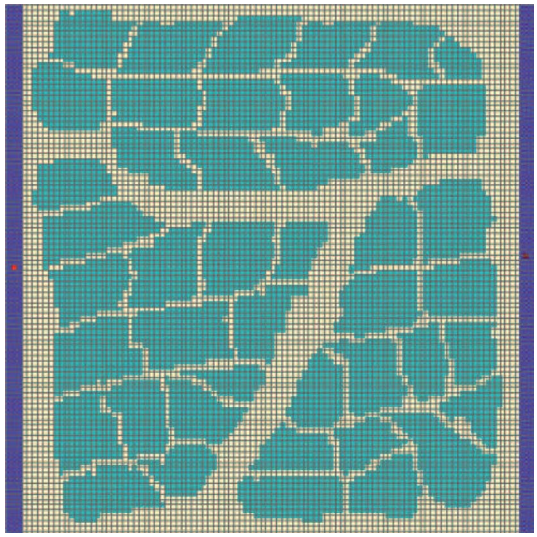

Fig. 11. Simulated structure resembling an actual tissue cut (100×100 squares, slice thickness $= 50\ \mu\text{m}$, pixel size $= 2\ \mu\text{m}$, membrane capacitance $= 1\ \mu\text{F/cm}^2$, plasma resistivity = cytoplasm resistivity $= 100\ \Omega\text{cm}$, electrode resistivity $= 0.001\ \Omega\text{cm}$)[68].

impedance of living tissues based on some numerical parameters concerning the tissue and bi-dimensional map representing a slice of the tissue [68]. An example of a simulated structure resembling an actual tissue from [68] is given in Fig. 11 representing three cell clusters separated by large extracellular spaces. The simulated impedance generated by *Bioimpedance Simulator* for this structure is very well represented by the single dispersion Cole impedance model.

There is a need to expand circuit simulation tools to include fractional order elements to simplify working with these models. Current methods require significant effort from measurement of fractional impedances to implementation of circuit models for simulation. Expanding these tools will remove the expertise required to implement approximated fractional order circuit models and encourage researchers to conduct simulations in the field of bioimpedance.

VII. Example Parameter Extraction

In this section, we present an example of extracting the single dispersion Cole impedance parameters from an impedance dataset using a nonlinear least squares fitting in MATLAB. The nonlinear least squares fitting attempts to solve the constrained optimization problem

$$\min_x \|Z(x) - ydata\|_2^2 = \min_x \sum_i^n (Z(x)_i - ydata_i)^2 \quad s.t. \quad x > 0 \tag{9}$$

where x is the vector of impedance parameters (R_∞, R_1 C_1, α_1), $Z(x)$ is the model impedance (3) calculated using x, $ydata$ is the collected impedance to fit to (3), $Z(x)_i$ and $ydata_i$ are the simulated and collected dataset at frequency ω_i, and n is the total number of data points in the collected dataset. This routine

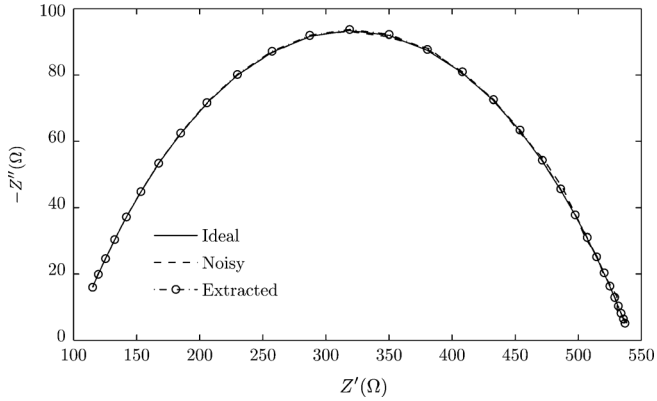

Fig. 12. MATLAB simulated ideal (solid), noisy (dashed), and extracted (circles) impedance plots of the single dispersion Cole impedance when $R_\infty = 98.2\ \Omega$, $R_1 = 443.9\ \Omega$, $C_1 = 2.551\ \mu\text{F}$, and $\alpha = 0.507$ from 30 Hz to 32 MHz.

aims to find the impedance parameters that would ideally reduce the least squares error to zero or realistically to the level of noise within the dataset. The constraint is added for this problem because negative resistances and capacitances are not physically possible and a negative value of α would indicate a fractional inductor not a fractional capacitor.

Using (3) an ideal impedance dataset was generated with parameters $R_\infty = 98.2\ \Omega$, $R_1 = 443.9\ \Omega$, $C_1 = 2.551\ \mu\text{F}$, and $\alpha = 0.507$ from 30 Hz to 32 MHz using 30 logarithmically spaced datapoints. The data used for the fitting routine was created by adding 1% noise to the ideal dataset. These ideal and noisy datasets are shown in Fig. 12 as solid and dashed lines, respectively. The impedance parameters were estimated from the noisy data using the MATLAB *lsqcurvefit* function with the trust-region-reflective algorithm [69]. This function iteratively solves for the impedance parameters from an initial set x_0. To increase the proximity of x_0 to the solution we can select values of R_∞ and R_1 from the impedance dataset knowing

$$Z(0) = R_\infty + R_1 \tag{10}$$

$$Z(\infty) = R_\infty. \tag{11}$$

Therefore, using a sufficiently low and high frequency impedance values we can approximate $R_\infty \approx Z'(y_n)$ and $R_1 \approx R_\infty - Z'(y_1)$ where Z' is the real component of the impedance dataset and $y_{1,n}$ are the first and last datapoints, respectively. Applied to the noisy dataset in Fig. 12 yields initial conditions $R_\infty \approx 115.56\ \Omega$ and $R_1 \approx 423.05\ \Omega$. Selecting $C_1 = 1\ \mu\text{F}$ and $\alpha_1 = 0.75$ based on values within the range reported in literature yields the initial condition $x_0 = [115.56, 423.05, 1\mu, 0.75]$. Using x_0 in (9) with the noisy dataset, yields parameters $R_\infty = 98.33\ \Omega$, $R_1 = 443.89\ \Omega$, $C_1 = 2.50\ \mu\text{F}$, and $\alpha_1 = 0.5086$ with relative errors of 0.1303%, 0.0033%, 2.0882%, and 0.3152%, respectively, compared to the ideal values. The simulated impedance using the extracted parameters is given in Fig. 12 as circles. This extraction process can be modified and applied to any of the fractional-order impedance models presented in this paper.

TABLE I
COMPARISON OF FRACTIONAL ORDER CIRCUIT MODELS USED IN BIOLOGY AND BIOMEDICINE

Schematic	Frequency Range	Impedance Plot	Tissue Types
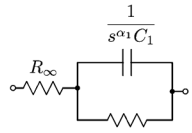 $Z(s) = R_\infty + \frac{R_1}{1+s^{\alpha_1}R_1C_1}$	30 Hz - 32 MHz	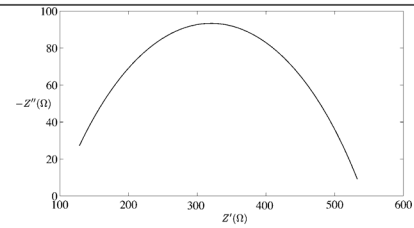 $R_\infty = 98.2\ \Omega$, $R_1 = 443.9\ \Omega$, $C_1 = 2.551\ \mu$F, $\alpha_1 = 0.507$	Organ Tissues [11], Human Blood [12], [13], Skull [17], Teeth [19], Full Body [16], [20], Fruits & Vegetables [35], [36], [41], Tree Cuttings [42], [45]
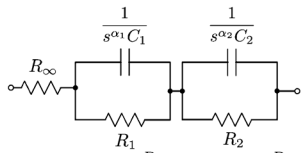 $Z(s) = R_\infty + \frac{R_1}{1+s^{\alpha_1}R_1C_1} + \frac{R_2}{1+s^{\alpha_2}R_2C_2}$	10 mHz - 10 MHz	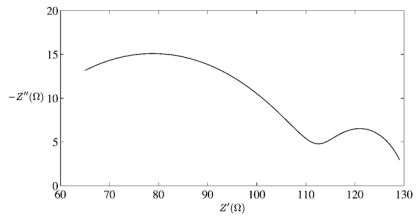 $R_\infty = 42.9\ \Omega$, $R_1 = 71.6\ \Omega$, $R_2 = 16.5\ \Omega$, $C_1 = 3.086\ \mu$F, $C_2 = 89.29\ \mu$F, $\alpha_1 = 0.507$, $\alpha_2 = 0.766$	Sheep Intestine [11], Tumor Xenografts [27], Teeth [28]
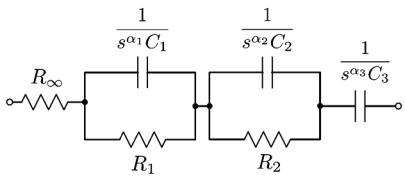 $Z(s) = R_\infty + \frac{R_1}{1+s^{\alpha_1}R_1C_1} + \frac{R_2}{1+s^{\alpha_2}R_2C_2} + \frac{1}{s^{\alpha_3}C_3}$	40 Hz - 340 kHz	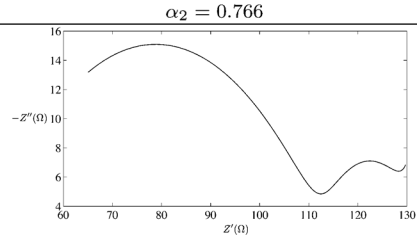 $R_\infty = 42.9\ \Omega$, $R_1 = 71.6\ \Omega$, $R_2 = 16.5\ \Omega$, $C_1 = 3.086\ \mu$F, $C_2 = 89.29\ \mu$F, $C_3 = 769\ \mu$F, $\alpha_1 = 0.507$, $\alpha_2 = 0.766$, $\alpha_3 = 0.9$	Root/Stem/Electrode Interface [47]
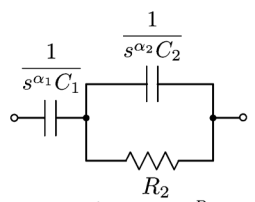 $Z(s) = \frac{1}{s^{\alpha_1}C_1} + \frac{R_2}{1+s^{\alpha_2}R_2C_2}$	1 kHz - 100 kHz	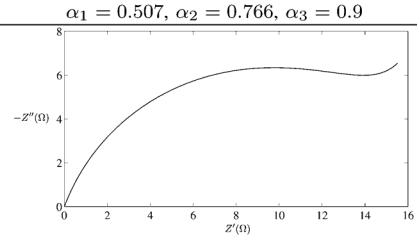 $R_2 = 16.5\ \Omega$, $C_1 = 769\ \mu$F, $C_2 = 89.29\ \mu$F, $\alpha_1 = 0.507$, $\alpha_2 = 0.766$	Wood tissue [48]
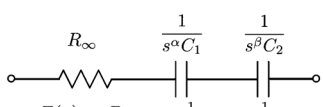 $Z(s) = R_\infty + \frac{1}{s^{\alpha}C_1} + \frac{1}{s^{\beta}C_2}$	6 kHz - 925 kHz	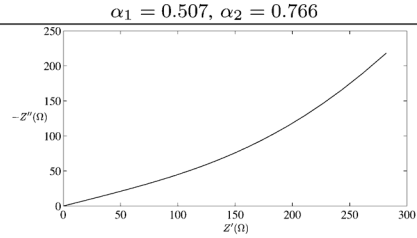 $R_\infty = 0$, $C_1 = 0.0071$ F, $C_2 = 0.1$ F, $\alpha_1 = 0.25$, $\alpha_2 = 0.875$	Electrode/Tissue Interface [52]
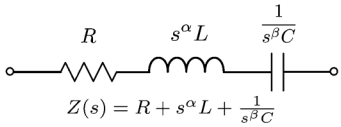 $Z(s) = R + s^{\alpha}L + \frac{1}{s^{\beta}C}$	4 Hz - 48 Hz	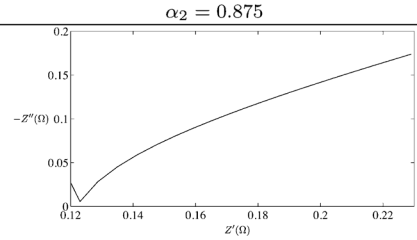 $R = 0.0147$, $L = 0.0193$, $C = 0.9921$, $\alpha = 0.4687$, $\beta = 0.7271$	Human Respiratory System [60], [62]

VIII. Model Comparison

An overview of all six models presented in this paper is given in Table I. This table compiles the schematic and impedance expression for each model, the frequency range over which each model is used in the literature, a simulated impedance loci of the model, and the types of tissues for which these models are used. Reviewing the impedance loci's of each model it can be seen that the parallel combination of a resistor and CPE in each model results in a depressed semi-circle. These depressed semi-circles are seen in the impedance plots of (3) and (6) with two each in the plots of (4) and (5). A series CPE contributes an upward hook at low frequencies in the impedance loci, which can be seen in the impedance plots of (5) and (6). We also see an extreme case of this upward hook in the impedance loci of (7) which has two series CPEs. Knowledge of how each component will contribute to the impedance plot of a fractional model is useful when determining which model to fit to experimental data.

IX. Conclusion

Fractional order circuit models provide a better fit for experimentally collected impedance data of biological tissues over their integer-order counterparts. These models, while lacking in providing a physiological explanation of the underlying mechanisms, are still very useful showing a wide array of applications in biomedicine and biology. The practical application of these models warrants significant continued research into not only their use as prognostic and diagnostic tools, but also into techniques for their measurement and software for their simulation.

References

[1] K. B. Oldham and J. Spanier, *The Fractional Calculus: Theory and Applications of Differentiation and Integration to Arbitrary Order*. New York, : Academic, 1974.

[2] M. D. Ortigueira, *Fractional Calculus for Scientists and Engineers*. Heidelberg, Germany: Springer, 2011.

[3] M. D. Ortigueira, "An introduction to the fractional continuous-time linear systems: the 21st century systems," *IEEE Circuits Syst. Mag.*, vol. 8, no. 3, pp. 19–26, Aug. 2008.

[4] A. S. Elwakil, "Fractional-order circuits and systems: An emerging interdisciplinary research area," *IEEE Circuits Syst. Mag.*, vol. 10, no. 4, pp. 40–50, 2010.

[5] R.L Magin, *Fractional Calculus in Bioengineering*. West Redding, CT: Begell House, 2006.

[6] I. Podlubny, *Fractional Differential Equations*. San Diego, CA: Academic, 1999.

[7] M. Nakagawa and K. Sorimachi, "Basic characteristics of a fractance device," *IEICE Trans. Fundam. Electron. Commun. Comput. Sci.*, vol. 75, pp. 1814–1819, 1992.

[8] S. Grimnesand and O. Martinsen, *Bioimpedance and Bioelectricity Basics*. New York: Academic, 2000.

[9] K. S. Cole, "Permeability and impermeability of cell membranes for ions," in *Proc. Cold Spring Harbor Symp. Quant. Biol.*, 1940, vol. 8, pp. 110–122.

[10] K. S. Cole and R. H. Cole, "Dispersion and absorption in dielectrics I. Alternating current characteristics," *J. Chem. Phys.*, vol. 9, pp. 341–351, 1941.

[11] B. Rigaud, L. Hamzaoui, M. R. Frikha, N. Chauveau, and J. P. Morucci, "In vitro tissue characterization and modelling using electrical impedance measurements in the 100 HZ—10 MHz frequency range," *Physiol. Meas.*, vol. 16, no. 3A, pp. A15–A28, 1995.

[12] Y. Ulgen and M. Sezdi, "Hematocrit dependence of the Cole-Cole parameters of human blood," *Int. Biomed. Eng. Days*, pp. 71–74, 1998.

[13] M. Sezdi, M. Bayik, and Y. Ulgen, "Storage effects on the Cole-Cole parameters of erythrocyte suspensions," *Physiol. Meas.*, vol. 27, no. 7, pp. 623–635, 2006.

[14] S. Kun, B. Ristic, and R. A. Peura, "Algorithm for tissue ischemia estimation based on electrical impedance spectroscopy," *IEEE Trans. Biomed. Eng*, vol. 50, no. 12, pp. 1352–1359, Dec. 2003.

[15] A. Ivorra, M. Genesca, A. Sola, L. Palacios, R. Villa, G. Hotter, and J. Aguilo, "Bioimpedance dispersion width as a parameter to monitor living tissues," *Physiol. Meas.*, vol. 26, no. 2, pp. S165–S173, 2005.

[16] O. I. Al-Surkhi, P. J. Riu, F. F. Vazquez, and J. Ibeas, "Monitoring Cole-Cole parameters during haemodialysis (HD)," in *IEEE Int. Conf. Eng. Med. Biol. Soc.*, 2007, pp. 2238–2241.

[17] C. Tang, F. You, G. Cheng, D. Gao, F. Fu, and X. Dong, "Modeling the frequency dependence of the electrical properties of the live human skull," *Physiol. Meas.*, vol. 30, no. 12, pp. 1293–1301, 2009.

[18] G. C. McConnell, R. J. Butera, and R. V. Bellamkonda, "Bioimpedance modeling to monitor astrocytic response to chronically implanted electrodes," *J. Neural Eng.*, vol. 6, no. 5, p. 055005, 2009.

[19] A. P. Morais, A. V. Pino, and M. N. Souza, "A fractional electrical impedance model in detection of occlusal non-cavitated carious," in *IEEE Int. Conf. Eng. Med. Biol. Soc.*, 2010, pp. 6551–6554.

[20] R. Buendia, R. Gil-Pita, and F. Seoane, "Cole parameter estimation from the modulus of the electrical bioimpedance for assessment of body composition. A full spectroscopy approach," *J. Electr. Bioimpedance*, vol. 2, pp. 72–78, 2011.

[21] A. J. Barrow and S. M. Wu, "Impedance measurements for cervical cancer diagnosis," *Gynecolog. Oncol.*, vol. 107, no. 1, pp. S40–S43, 2007.

[22] S. Laufer, A. Ivorra, V. E. Reuter, B. Rubinsky, and S. B. Solomon, "Electrical impedance characterization of normal and cancerous human hepatic tissue," *Physiol. Meas.*, vol. 31, no. 7, pp. 995–1009, 2010.

[23] W. D. Gregory, J. J. Marx, G. W. Gregory, W. M. Mikkelson, J. A. Tjoe, and J. Shell, "The Cole relaxation frequency as a parameter to identify cancer in breast tissue," *Med. Phys.*, vol. 39, no. 7, pp. 4166–4174, 2012.

[24] C. Wang, M. Li, and M. Yao, "Impedance feature extraction of breast cancer and surrounding tissues," in *Proc. Int. Conf. Biomed. Eng. Inf.*, 2010, pp. 922–926.

[25] A. Keshtkar, Z. Salehnia, A. Keshtkar, and B. Shokouhi, "Bladder cancer detection using electrical impedance technique (tabriz mark 1)," *Pathol. Res. Int.*, vol. 2012, 2012.

[26] M. J. Tuorkey, "Bioelectrical impedance as a diagnostic factor in the clinical practice and prognostic factor for survival in cancer patients: prediction, accuracy and reliability," *J. Biosens. Bioelectron.*, vol. 4, no. 4, 2012.

[27] D. A. McRae, M. A. Esrick, and S. C. Mueller, "Changes in the noninvasive, in vivo electrical impedance of three xenografts during the necrotic cell-response sequence," *Int. J. Radiat. Oncol. Biol. Phys.*, vol. 43, no. 4, pp. 849–857, 1999.

[28] A. H. Eldarrat, D. J. Wood, G. M. Kale, and A. S. High, "Age-related changes in ac-impedance spectroscopy studies of normal human dentine," *J. Mater. Sci.: Mater. Med.*, vol. 18, no. 6, pp. 1203–1210, 2007.

[29] J. R. MacDonald, LEVM/LEVMW ver. 8.12, Aug. 2012 [Online]. Available: http://www.jrossmacdonald.com/levminfo.html

[30] MATLAB ver. 7.14.0, MathWorks, Mar. 1, 2012 [Online]. Available: http://www.mathworks.com

[31] L. C. Ward, T. Essex, and B. H. Cornish, "Determination of Cole parameters in multiple frequency bioelectrical impedance analysis using only the measurement of impedances," *Physiol. Meas.*, vol. 27, no. 9, pp. 839–850, 2006.

[32] D. Ayllon, F. Seoane, and R. Gil-Pita, "Cole equation and parameter estimation from electrical bioimpedance spectroscopy measurements—A comparative study," in *IEEE Int. Conf. Eng. Med. Biol. Soc.*, 2009, pp. 3779–3782.

[33] T. J. Freeborn, B. Maundy, and A. Elwakil, "Improved Cole-Cole parameter extraction from frequency response using least squares fitting," in *Proc. IEEE Int. Symp. Circuits Syst.*, 2012, pp. 337–340.

[34] T. J. Freeborn, B. Maundy, and A. Elwakil, "Least squares estimation technique of Cole-Cole parameters from step response," *Electron. Lett.*, vol. 48, no. 13, pp. 752–754, 2012.

[35] A. S. Elwakil and B. Maundy, "Extracting the Cole-Cole impedance model parameters without direct impedance measurement," *Electron. Lett.*, vol. 46, no. 20, pp. 1367–1368, 2010.

[36] B. Maundy and A. S. Elwakil, "Extracting single dispersion Cole-Cole impedance model parameters using an integrator setup," *Analog Integr. Circ. Sig. Process*, vol. 71, pp. 107–110, 2012.

[37] A. S. Elwakil and B. Maundy, "Experimental technique for estimating the dispersion coefficient of a constant phase element," in *Proc. Eur. Conf. Circuit Theory Des.*, 2011, pp. 469–471.
[38] H. Solmaz, Y. Ulgen, and M. Tumer, "Design of a micro-controller based Cole-Cole impedance meter for testing biological tissues," *World Congr. Med. Phys. Biomed. Eng.*, pp. 488–491, 2009.
[39] J. Ferreira, F. Seoane, and K. Lindecrantz, "Ad5933-based electrical bioimpedance spectrometer towards textile-enabled applications," in *Proc. IEEE. Int. Conf. Eng. Med. Biol. Soc.*, 2011, pp. 3282–3285.
[40] I. S. Jesus and J. A. T. Machado, "Application of integer and fractional models in electrochemical systems," *Math. Prob. Eng.*, vol. 2012, 2012.
[41] I. S. Jesus, J. A. T. Machado, and J. B. Cunha, "Fractional electrical impedances in botanical elements," *J. Vib. Control*, vol. 14, no. 9–10, pp. 1389–1402, 2008.
[42] S. Mancuso, "Seasonal dynamics of electrical impedance parameters in shoots and leaves relate to rooting ability of olive olea europaea cuttings," *Tree Physiol.*, vol. 19, no. 2, pp. 95–101, 1998.
[43] L. Wu, Y. Ogawa, and A. Tagawa, "Electrical impedance spectroscopy analysis of eggplant pulp and effects of drying and freezing-thawing treatments on its impedance characteristics," *J. Food Eng.*, vol. 87, no. 2, pp. 274–280, 2007.
[44] M. Tiitta *et al.*, "Spectral and chemical analyses of mould development on Scots pine hardwood," *Eur. J. Wood Prod.*, vol. 67, no. 2, pp. 151–158, 2009.
[45] T. Repo and M. I. N. Zhang, "Modelling woody plant tissues using a distributed electrical circuit," *J. Exp. Bot.*, vol. 44, no. 5, pp. 977–982, 1993.
[46] T. Repo, G. Zhang, A. Ryyppo, and R. Rikala, "The electrical impedance spectroscopy of Scots pine Pinus syvestris L. Shoots in relation to cold acclimation," *J. Exp. Bot.*, vol. 51, no. 353, pp. 2095–2107, 2000.
[47] T. Repo, J. Laukkanen, and R. Silvennoinen, "Measurement of the tree root growth using electrical impedance spectroscopy," *Silva Fennica*, vol. 39, no. 2, pp. 159–166, 2005.
[48] M. Tiitta and H. Oikkonen, "Electrical impedance spectroscopy device for measurement of moisture gradients in wood," *Rev. Sci. Instrum.*, vol. 73, no. 8, pp. 3093–3100, 2002.
[49] Y. Yamamoto, H. Harada, K. Yasuhara, and T. Nakamura, "Automatic sensing device of electrical characteristics of living trees," *IEEE Trans. Instrum. Meas.*, vol. 44, no. 3, pp. 729–733, Jun. 1995.
[50] C. Lin, L. Chen, and T. Chen, "The development and application of an electrical impedance spectroscopy measurement system for plant tissues," *Comput. Electron. Agric.*, vol. 82, pp. 96–99, 2012.
[51] M. Ovadia and D. H. Zavitz, "The electrode-tissue interface in living heart: Equivalent circuit as a function of surface area," *Electroanalysis*, vol. 10, no. 4, pp. 262–272, 1998.
[52] R. L. Magin and M. Ovadia, "Modelling the cardiac tissue electrode interface using fractional calculus," *J. Vib. Control*, vol. 14, no. 9–10, pp. 1431–1442, 2008.
[53] M. Ovadia, E. Fayn, and D. H. Zavitz, "Impedance experimentation for an electrode interface in human fetal tissue: Novel pathological regime of anomalous diffusion," *Chem. Phys. Lett.*, vol. 424, no. 4–6, pp. 285–288, 2006.
[54] B. West, *Fractal Physiology and Chaos in Medicine*. Singapore: World Scientific, 1990.
[55] J. Gao, Y. Cao, W. Tung, and J. Hu, *Multiscale Analysis of Complex Time Series*. : Wiley-Interscience, 2007.
[56] A. Oustaloup, *La Derivation non Entiere: Theorie, Sythese et Applications*, E. Hermes, Ed. Paris, France: , 1995.
[57] Z. Hantos, B. Daroczy, B. Suki, S. Nagy, and J. Fredberg, "Input impedance and peripheral inhomogeneity of dog lungs," *J. Appl. Physiol.*, vol. 72, no. 1, pp. 168–178, 1992.
[58] Z. Hantos, A. Adamicz, E. Govaerts, and B. Daroczy, "Mechanical impedances of lungs and chest wall in the cat," *J. Appl. Physiol.*, vol. 73, no. 2, pp. 427–433, 1992.
[59] C. M. Ionescu and R. D. Keyser, "Time domain validation of a fractional order model for human respiratory system," in *Proc. IEEE Mediter. Electrotechn. Conf.*, 2008, pp. 89–95.
[60] C. M. Ionescu and R. D. Keyser, "Relations between fractional-order model parameters and lung pathology in chronic obstructive pulmonary disease," *IEEE Trans. Biomed. Eng.*, vol. 56, no. 4, pp. 978–987, Apr. 2009.
[61] C. M. Ionescu, I. Muntean, J. A. Tenreiro-Machado, R. D. Keyser, and M. Abrudean, "A theoretical study on modelling the respiratory tract with ladder networks by means of intrinsic fractal geometry," *IEEE Trans. Biomed. Eng.*, vol. 57, no. 2, pp. 246–253, Feb. 2010.
[62] A. Beaulieu *et al.*, "Measurement of fractional order model parameters of respiratory mechanical impedance in total liquid ventilation," *IEEE Trans. Biomed. Eng.*, vol. 59, no. 2, pp. 323–331, Feb. 2012.
[63] D. Stancic, J. Q. Fang, and I. Cosic, "Distributed biological tissue impedance model for SPICE simulation," in *Proc. Int. Symp. Bioelectron. Bioinf.*, 2009, pp. 201–205.
[64] J. Valsa and J. Vlach, "RC models of a constant phase element," *Int. J. Circ. Theor.*, 2011.
[65] I. Podlubny, I. Petras, B. Vinagre, P. O'Leary, and L. Dorcak, "Analgoue realizations of fractional-order controllers," *Nonlinear Dyn.*, vol. 29, no. 1–4, pp. 281–296, 2002.
[66] B. Krishna and K. Reddy, "Active and passive realization of fractance device of order 1/2," *Act. Passive Electron. Compon.*, 2008.
[67] A. Ivorra, BioZsim [Online]. Available: http://www.cnm.es/~mtrans/BioZsim/
[68] A. Ivorra, R. Gomez, and J. Aguilo, "A SPICE netlist generator to simulate living tissue electrical impedance," in *Proc. Int. Conf. Electr. Bioimpedance*, 2004, pp. 317–320.
[69] T. Coleman and Y. Li, "An interior, trust region approach for nonlinear minimization subject to bounds," *SIAM J. Optim.*, vol. 6, pp. 418–445, 1996.

Todd J. Freeborn received the B.Sc. and M.Sc. degrees, in 2008 and 2010, respectively, from the University of Calgary, Calgary, AB, Canada, where he is currently working toward the Ph.D. degree in electrical engineering.

His research interests include the investigation of fractional-order circuits and systems, specifically in fractional-step analog filters for signal processing and the indirect measurement of fractional impedances.